



1 The Impact of Increasing Stratospheric Radiative Damping on the QBO Period

2 Tiehan Zhou^{1,2}, Kevin DallaSanta^{1,3}, Larissa Nazarenko^{1,2}, Gavin A. Schmidt¹

3 ¹NASA Goddard Institute for Space Studies, New York, NY

4 ²Center for Climate Systems Research, Columbia University, New York, NY

5 ³Universities Space Research Association, Columbia, MD

6

7 Correspondence to: Tiehan Zhou (tz2131@columbia.edu)

8

9

10 **Abstract.** Stratospheric radiative damping increases as atmospheric carbon dioxide concentration rises.

11 We use the one-dimensional mechanistic models of the QBO to conduct sensitivity experiments and

12 find that when atmospheric carbon dioxide concentration increases, the simulated QBO period shortens

13 due to the enhancing of radiative damping in the stratosphere. This result suggests that increasing

14 stratospheric radiative damping due to rising CO₂ may play a role in determining the QBO period in a

15 warming climate along with wave momentum flux entering the stratosphere and tropical vertical

16 residual velocity, both of which also respond to increasing CO₂.

17

18 1. Introduction

19 The quasi-biennial oscillation (QBO) dominates the variability of the equatorial middle and lower

20 stratosphere and is characterized by a downward propagating zonal wind regime that regularly changes

21 from westerlies to easterlies. The QBO period ranges from 22 to 34 months with its average being

22 slightly longer than 28 months. The QBO not only manifests itself in the equatorial zonal winds, but also

23 leaves an imprint on the temperature in both the tropics and extratropics (Baldwin et al., 2001 and

24 references therein).

25 The QBO has far-reaching implications for global weather and climate systems. First of all, the QBO

26 exerts a marked influence on the distribution and transport of various chemical constituents such as



27 ozone (O_3) (e.g., Hasebe, 1994), water vapor (H_2O) (e.g., Kawatani et al., 2014), methane (CH_4), nitrous
28 oxide (N_2O), hydrogen fluoride (HF), hydrochloric acid (HCl), odd nitrogen species (NO_y) (e.g.,
29 Zawodny and McCormick, 1991), and volcanic aerosol (Trepte and Hitchman, 1992). Secondly, it is
30 well appreciated that the QBO influences the extratropical circulation in the winter stratosphere, which
31 is commonly known as the Holton–Tan effect (Holton and Tan, 1980; Labitzke, 1982). It has been noted
32 that the effect of the QBO on the extratropical winter stratosphere impacts the severity of stratospheric
33 ozone depletion (e.g., Lait et al., 1989). Furthermore, taking account of the QBO improves the simulation
34 and predictability of the extratropical troposphere (e.g., Marshall and Scaife, 2009). Finally, through its
35 modulation of temperature and vertical wind shear in the vicinity of the tropical tropopause, the QBO
36 influences tropical moist convection (Collimore et al., 2003; Liess and Geller, 2012), the El Niño–
37 Southern Oscillation (ENSO) (Gray et al., 1992; Huang et al., 2012; Hansen et al. 2016), the Hadley
38 circulation (Hitchman and Huesmann, 2009), the tropospheric subtropical jet (Garfinkel and Hartmann,
39 2011a, 2011b), the boreal summer monsoon (Giorgetta et al., 1999), and the Madden-Julian Oscillation
40 (Yoo and Son, 2016). Intriguingly, the QBO is also reported to influence the activities of tropical
41 cyclones (Gray et al., 1984; Ho et al., 2009), albeit this issue is still unsettled (Camargo and Sobel, 2010)
42 and needs further study.

43 Efforts to understand and simulate the QBO have been ongoing ever since its discovery by Ebdon
44 (1960) and Reed et al. (1961). Lindzen and Holton (1968) and Holton and Lindzen (1972) developed
45 the classical theory of the QBO. Namely, as waves propagate upward, they are attenuated by thermal
46 damping, encounter critical levels, and accelerate and decelerate the mean flow, providing momentum
47 sources for both the westerly and easterly phases of the QBO.

48 Holton and Lindzen’s (1972) model (hereafter referred to as HL model) was further simplified by
49 Plumb (1977), the elegance of which made it a standard paradigm for the QBO. In Plumb’s (1977)



50 Boussinesq formulation, the QBO period is inversely dependent upon both the momentum flux and
51 thermal dissipation rate. Hamilton (1981) further highlighted the role of the radiative damping rate on
52 both the realistic vertical structure and the realistic period of the QBO.

92 By adopting higher vertical resolutions and incorporating various gravity wave parameterization
93 schemes, many state-of-the-art climate models have shown the capability to self-consistently simulate
94 the QBO (Scaife et al., 2000; Giorgetta et al., 2002, 2006; Rind et al., 2014, 2020; Geller et al., 2016;
95 Richter et al., 2020a, 2020b). Given the important implications of the QBO for the global climate system,
96 it is natural to ask how the QBO will change in a warming climate.

97 Giorgetta and Doege (2005) showed a shortening of the QBO period in their doubled CO₂
98 experiments. They reasoned that both the weakening of the tropical upwelling and the prescribed
99 increase of gravity wave sources lead to the reduction of the QBO period in a warming climate. However,
100 most climate models project a strengthening rather than weakening of tropical upwelling in a warmer
101 climate (Butchart et al., 2006, 2014; Li et al., 2008). Employing a model without any parametrized non-
102 orographic gravity waves, Kawatani et al. (2011) demonstrated that the intensifying tropical upwelling
103 in a warming climate dominates the counteracting effect of enhanced wave fluxes and consequently
104 projected a lengthening of the QBO period. Using fixed sources of parametrized gravity waves,
105 Watanabe and Kawatani (2012) also projected the QBO longer period in a warming climate and pointed
106 out that the lengthening of the QBO is due to the stronger tropical upwelling. Analyzing four Coupled
107 Model Intercomparison Project phase 5 (CMIP5) models that could simulate a reasonable QBO,
108 Kawatani and Hamilton (2013) found that the projected trends of the QBO period were inconsistent in
109 sign. They further investigated the 60-year operational balloon-borne radiosonde observations provided
110 by the Free Berlin University and detected no significant trend in the QBO period. Richter et al. (2020b)
111 investigated the response of the QBO in a doubled and quadrupled CO₂ climate among eleven models



112 that participated in Phase 1 of the Stratospheric-tropospheric Processes And their Role in Climate QBO-
113 initiative (QBOi; Butchart et al., 2018), and found no consensus on how the QBO period would respond
114 to a changing climate. Recently, Butchart et al. (2020) evaluated ten Coupled Model Intercomparison
115 Project phase 6 (CMIP6) models with realistic QBO in two Shared Socioeconomic Pathways (SSPs,
116 Gidden et al., 2019) scenario simulations and surprisingly found that the QBO period shortens in seven
117 of those ten models in both in both SSP3-7.0 and SSP5-8.5 scenarios although only two and three models
118 show a significant shortening trend in the respective scenarios.

119 It is challenging to ascertain the trend of the QBO period in a warming climate. On one hand, a
120 speeding-up of the Brewer-Dobson circulation in a warming climate leads to a lengthening of the QBO
121 period in most climate models. On the other hand, there is a robust increase in the vertical component of
122 the EP flux for both eastward and westward propagating waves (Richter et al., 2020b; Butchart et al.,
123 2020), indicating that the QBO period shortens due to the enhanced wave driving in a warming climate.
124 The competing effects between enhanced wave driving and a faster Brewer-Dobson circulation suggests
125 that trends in the QBO period are likely to be small and difficult to detect due to the large cycle-to-cycle
126 variability that is reproduced by climate models (Butchart et al., 2020). In addition, uncertainty in the
127 representation of the parameterized gravity waves make it more elusive to detect the trend of the QBO
128 period in a warming climate (Schirber et al., 2015; Richter et al., 2020b).

129 Given the fact that the QBO period is influenced by the radiative damping (Plumb 1977; Hamilton
130 1981), a natural question to ask is whether it could play a role on the trend of the QBO in a warming
131 climate. Plass (1956) showed that when the CO₂ concentration is increased from 330 ppmv to 660 ppmv,
132 the cooling rate increases significantly in the middle and upper stratosphere while it is not changed below
133 the 24 km height level. The cooling rate is increased by more than 50% around the 40 km height level
134 (see his Figure 8).



135 It is well-known that enhanced wave fluxes entering the stratosphere and stronger tropical upwelling
136 individually play a dominant role in determining the trends in the QBO period in a warming climate.
137 Does the competing effect between them leave some room for increasing stratospheric radiative damping
138 to exert an influence on the QBO period? In this paper, we use the HL model to isolate the effect of
139 radiative damping on the QBO period by assuming that the momentum flux entering the stratosphere
140 doesn't change in our experiments. Observational and modeling studies (Andrews et al., 1987; Kawatani
141 et al., 2009, 2010, 2011; Richter et al., 2020b; Holt et al., 2020) showed that the wave forcing spectrum
142 is similar to a discrete two-wave spectrum rather than red-noise or white-noise, all of which are
143 illustrated in Saravanan (1990). Accordingly, the QBO is indeed sensitive to stratospheric radiative
144 damping, and the HL model is suitable for us to conduct the sensitivity test.

145 The remainder of this paper is organized as follows. Section 2 investigates the sensitivity of the QBO
146 period to the radiative damping using HL's original model. Section 3 explores the sensitivity of the QBO
147 period to the radiative damping using a modified HL model where the semiannual forcing is removed.
148 Discussion and conclusions are presented in Sections 4 and 5 respectively.

149

150 **2. Sensitivity of the QBO period to enhanced stratospheric radiative damping in the original HL** 151 **model**

152 In the HL model the governing equation of mean flow emerges after the primitive momentum
153 equation is meridionally averaged over some suitable latitudinal belt over the equator.

$$154 \quad \frac{\partial \bar{u}}{\partial t} = -\frac{1}{\rho_0} \frac{\partial}{\partial z} \left[\sum_{i=0}^1 \bar{F}_i \right] + K_z \frac{\partial^2 \bar{u}}{\partial z^2} + G \quad (1)$$



155 where \bar{u} is mean zonal wind, ρ_0 is mean density, \bar{F}_i is the meridionally averaged vertical Eliassen-Palm
156 flux associated with wave i , the index i refers to the individual waves, K_z is a vertical eddy diffusion
157 coefficient, t is time, z is altitude, and G is semiannual forcing identical to that specified by HL.

158 The \bar{F}_i is are evaluated with Lindzen's (1971) WKB formalism for equatorial waves in shear. When
159 only infrared cooling acts to damp the waves the formulae for \bar{F}_i are

$$160 \quad \bar{F}_0(z) = A_0 \exp\left(-\int_{17km}^z \frac{\alpha N}{k(c-\bar{u})^2} dz\right) \quad (2)$$

161 for the Kelvin wave, and

$$162 \quad \bar{F}_1(z) = A_1 \exp\left[-\int_{17km}^z \frac{\alpha\beta N}{k^3(c-\bar{u})^3} \left(1 - \frac{k^2(\bar{u}-c)}{\beta}\right) dz\right] \quad (3)$$

163 for the mixed Rossby-gravity wave. As in HL, the wavenumber k , the phase speed c , and A_0 are chosen
164 to be $2\pi/(40,000 \text{ km})$, 30 m s^{-1} , and $0.04 \text{ m}^2 \text{ s}^{-2} \rho_0(17 \text{ km})$, respectively for the Kelvin wave while
165 they are equal to $-2\pi/(10,000 \text{ km})$, -30 m s^{-1} , and $-0.04 \text{ m}^2 \text{ s}^{-2} \rho_0(17 \text{ km})$, respectively for the
166 mixing Rossby-gravity wave. In Eq. (1), $K_z = 0.3 \text{ m}^2 \text{ s}^{-1}$, which is also the same as in HL. In addition,
167 $\beta = 2\Omega/a$, where Ω is earth's rotation rate, and a is earth's radius. HL's boundary conditions stipulated
168 that $\bar{u} = 0$ at the lowest model level (17 km) and constrained \bar{u} to vary semiannually at the top level (35
169 km).

170 In our control run that is used to depict the present-day QBO all the model parameters are identical
171 to those used by HL in their original simulation. The Brunt-Väisälä frequency

$$172 \quad N = \sqrt{\frac{g}{T_0} \left(\frac{dT_0}{dz} + \frac{g}{c_p} \right)} \quad (4)$$

173 In Eq. (4), g is gravity, T_0 is mean temperature, and c_p is specific heat of dry air at constant pressure.
174 HL set N in Eq. (4) to $2.16 \times 10^{-2} \text{ s}^{-1}$ with a scale height $H = 6 \text{ km}$. In addition, the Newtonian



175 cooling profile in our control run, i.e., $\alpha(z)$ in Eqs. (2) and (3), is also identical to that in the original
176 HL model and depicted in FIG. 1 as the black line. Namely, $\alpha(z)$ in the control run increases from
177 $(21 \text{ day})^{-1}$ at 17 km to $(7 \text{ day})^{-1}$ at 30 km and is kept at $(7 \text{ day})^{-1}$ between 30 km and 35 km. Fels
178 (1985) explicated why this cooling rate is suitable for simulating the QBO on the basis of the scale-
179 dependent effect of radiative damping (Fels 1982). Hamilton (1981) demonstrated that the proper choice
180 of $\alpha(z)$ is crucial in simulating a realistic vertical structure of the QBO.

181 Eq. (1) was integrated for 100 years using the forward-backward scheme (Matsuno, 1966). The
182 vertical resolution was 250 m and identical to that in HL. The time step was 12 hr, i.e., one half of used
183 in HL, because the 24-hr time step resulted in numerical instability in our integration.

184 FIG. 2a shows the time–height section of the monthly averaged mean zonal wind simulated over the
185 first 20 years using the HL model. Both the QBO and the semiannual oscillation (SAO) are conspicuous.
186 The fast Fourier transform (FFT) method is used to calculate the frequency power spectra. In order to
187 more accurately derive the QBO period, the model was run for 100 years to increase the spectral
188 resolution. Frequency–height sections of the power spectral densities (PSD) over zero to the Nyquist
189 frequency, i.e., 0.5 cycle/month, depict two sharp lines (peaks) at $\frac{1}{30}$ and $\frac{1}{6}$ cycle/month, respectively
190 (not shown). In order to better visualize the magnitudes of the PSD, we show two truncated frequency–
191 height sections with FIG. 2b and FIG. 2c highlighting the QBO and the SAO respectively. FIG. 2b shows
192 that the QBO dominates over the model domain. The peak frequency corresponds to the period of 30
193 months. FIG. 2c shows the SAO dominates near the model top due to the fact a semiannual forcing was
194 imposed in the altitudes from 28 to 35 km.

195 It is worth mentioning that the QBO period shown here is longer than 26.5 months reported in the HL
196 paper (see their FIG. 1). Using the HL model parameters, the QBO period simulated by Plumb (1977)
197 was close to three years (refer to his FIG. 8a), which is longer than our simulated QBO period, i.e., 30.0



198 months. Although we could not explain why our simulated QBO period is longer than that simulated by
199 HL, we found that when the upper boundary condition is changed from $\bar{u} = 14 \sin(\omega_a t)$ and $\omega_a =$
200 $\frac{2\pi}{180} \text{ day}^{-1}$ used in the HL's original model (refer to their Eqs. (2)) to $\frac{\partial \bar{u}}{\partial z} = 0$ used in Plumb (1977), the
201 simulated QBO period becomes 34.3 month (figure not shown). In other words, when we adopted the
202 stress-free upper boundary condition as in Plumb (1977), our simulated QBO period is comparable to
203 that simulated by him, which lends credence to our reconstruction of the HL model.

204 As mentioned in Section 1, when the atmospheric carbon dioxide concentration is doubled the cooling
205 rate increases significantly in the middle and upper stratosphere while it is not changed below the 24 km
206 height level. The cooling rate is increased by more than 50% around the 40 km height level (Plass, 1956).
207 Accordingly, the Newtonian cooling profile in our experimental run, i.e., $\alpha(z)$ in Eqs. (2) and (3), is
208 specified in FIG. 1 as the red line. Namely, $\alpha(z)$ in the experimental run increases from $(21 \text{ day})^{-1}$ at
209 17 km to $\frac{9}{91} \text{ day}^{-1}$ at 24 km, which is identical to that in the control run from 17 km to 24 km. We
210 increased $\alpha(z)$ in the experimental run between 30 km and 35 km by 30% relative to that in the control
211 run. In other words, $\alpha(z)$ is kept at $\frac{1.3}{7} \text{ day}^{-1}$ between 30 km and 35 km in the experimental run. The
212 percentage increase in $\alpha(z)$ for the doubled CO_2 above 30 km shown in FIG. 1 is comparable to that
213 shown by Plass (1956) in his Figure 8. Between 24 km and 30 km, $\alpha(z)$ in the experimental run is
214 formulated linearly with height from $\frac{9}{91} \text{ day}^{-1}$ at 24 km to at $\frac{1.3}{7} \text{ day}^{-1}$ at 30 km.

215 In order to properly investigate the sensitivity of the QBO period to enhanced stratospheric radiative
216 damping in response to the doubled CO_2 , it is worth mentioning that both α and N in Eqs. (2) and (3)
217 change with increasing CO_2 . Richter et al. (2020b) showed that N^2 would be decreased by $\sim 5\%$ in the
218 stratosphere when CO_2 is doubled (refer to their Figure 2c). Accordingly, the Brunt-Väisälä frequency
219 in the following experimental run, i.e., N in Eqs. (2) and (3), was decreased by $\sim 2.5\%$ compared with



220 that in the previous control run. FIG. 3a shows the time–height section of the monthly averaged mean
221 zonal wind simulated over the first 20 years for the doubled CO₂ run. Obviously, the QBO dominates
222 below 28 km while the semiannual oscillation (SAO) dominates above 31 km. Like FIG. 2b and FIG. 2c,
223 we only show two truncated frequency–height sections with FIG. 3b highlighting the QBO and FIG. 3c
224 highlighting the SAO. FIG. 3b also shows that the QBO dominates over the model domain. The peak
225 frequency corresponds to the period of 28.6 months. FIG. 3c shows the SAO dominates near the model
226 top due to the same imposed semiannual forcing as that in the control run.

227 In summary, using the original HL model we found that the increased radiative damping due to the
228 doubling of CO₂ shortens the QBO period by 4.7%.

229

230 **3. Sensitivity of the QBO period to enhanced stratospheric radiative damping in the HL model** 231 **without the semiannual forcing**

232 HL pointed out that the imposed semiannual oscillation was not essential for their QBO theory.
233 Applying $\frac{\partial \bar{u}}{\partial z} = 0$ as the upper boundary condition, Plumb (1977) showed a simulated QBO without
234 resorting to the semiannual momentum source (refer to his FIG. 8b). In the following control run, all
235 parameters are identical to those used in the previous control run in section 2 except that G in Eq. (1) is
236 set to zero with $\frac{\partial \bar{u}}{\partial z}$ also being set to zero at $z = 35$ km. Hereafter we refer to it as the Plumb model¹. FIG.
237 4a shows the time–height section of the monthly averaged mean zonal wind simulated over the first 20
238 years using the Plumb model. As expected, the QBO emerges without any trace of SAO since $G = 0$ in
239 Eq. (1). FIG. 4b shows that the QBO dominates over the whole model domain. The peak frequency
240 corresponds to the period of 37.5 months, which is comparable to that simulated by Plumb (1977) shown

¹ Strictly speaking, it is the HL model modified by Plumb (1977). In this paper, we don't use his eponymous model, i.e., the simplest possible model of the QBO, where Boussinesq fluids with uniform mean density were employed, because the HL model and its variant are considerably more realistic.



241 in his FIG. 8b. Apparently, the QBO period from the Plumb model, i.e., 37.5 months shown in FIG. 4b,
242 is longer than that from the HL model, i.e., 30.0 months shown in FIG. 2b because the additional forcing
243 G in Eq. (1) was removed in the Plumb model.

244 In the following experimental run, all parameters are identical to those used in the previous
245 experimental run in section 2 except that G in Eq. (1) is set to zero with $\frac{\partial \bar{u}}{\partial z}$ also being set to zero at $z =$
246 35 km. In other words, the following experimental run using the Plumb model employed the same
247 parameters as the afore-mentioned control run using the Plumb model with the following two exceptions.
248 Namely, the increased $\alpha(z)$ shown as the red line in FIG. 1 was used in the following experimental run
249 while $\alpha(z)$ shown as the black line in FIG. 1 was used in the above control run. In addition, the Brunt-
250 Väisälä frequency, i.e., N in Eqs. (2) and (3), was decreased by 2.5% in the following experimental run
251 compared with that in the above control run. FIG. 5a shows the time–height section of the monthly
252 averaged mean zonal wind simulated over the first 20 years for the doubled CO₂ run. It is natural that
253 only the QBO emerges. A comparison of FIG. 4a and FIG. 5a shows that the QBO period shortens when
254 the infrared damping increases in response to the doubled CO₂. FIG. 5b shows that the QBO dominates
255 over the whole model domain. The peak frequency corresponds to the period of 31.6 months.

256 Using the Plumb model, we found that the increased radiative damping due to the doubling of CO₂
257 shortens the QBO period by 15.7%.

258

259 4. Discussion

260 The semiannual forcing, G in Eq. (1), in the HL model is imposed rather than results from the wave-
261 flow interaction. In other words, G in Eq. (1) is independent of mean flow, and is specified as $G =$
262 0 for $z \leq 28$ km, and $G = \omega_{sa} \bar{u}_{sa}$ for $z > 28$ km



263 where $\bar{u}_{sa} = 2(z - 28\text{km}) \text{ m s}^{-1} \text{ km}^{-1} \sin(\omega_{sa}t)$ and $\omega_{sa} = \frac{2\pi}{180} \text{ day}^{-1} \approx 4 \times 10^{-7} \text{ s}^{-1}$ (refer to
264 Eqs. (2) in HL). Therefore, we have $\frac{\partial^2 \bar{u}_{sa}}{\partial z^2} = 0$ in the HL original model. We furthermore decompose \bar{u}
265 into two components: \bar{u}_{QBO} and \bar{u}_{sa} . Combining Eq. (1), the decomposition of \bar{u} as $\bar{u} = \bar{u}_{QBO} + \bar{u}_{sa}$,
266 the above-mentioned $\frac{\partial^2 \bar{u}_{sa}}{\partial z^2} = 0$, and $G = \omega_{sa} \bar{u}_{sa} = \frac{\partial \bar{u}_{sa}}{\partial t}$ for $z > 28 \text{ km}$, yields

$$267 \quad \frac{\partial \bar{u}_{QBO}}{\partial t} = -\frac{1}{\rho_0} \frac{\partial}{\partial z} \left[\sum_{i=0}^1 \bar{F}_i \right] + K_z \frac{\partial^2 \bar{u}_{QBO}}{\partial z^2} \quad (5)$$

268 for $z > 28 \text{ km}$.

269 Dunkerton (1997) showed that in the presence of tropical upwelling it was gravity waves rather than
270 large-scale Kelvin and mixed Rossby-gravity waves that contributed the bulk of QBO forcing.
271 Consequently, Geller et al. (2016a, 2016b) pointed out that enough gravity wave momentum flux is
272 required to model the QBO in a self-consistent manner in climate models and that the magnitude of the
273 subgrid-scale gravity wave momentum flux plays a crucial role in determining the QBO period. Since
274 there is no tropical upwelling in either the HL model or the Plumb model, and the semiannual forcing,
275 G , is dependent on neither \bar{u} in Eq. (1) nor \bar{u}_{QBO} in Eq. (5), it is natural that planetary-scale Kelvin and
276 mixed Rossby-gravity waves largely determine the QBO periods shown in Sections 2 and 3 due to the
277 fact that G only exerts a weak influence on the planetary wave forcing, i.e., $-\frac{1}{\rho_0} \frac{\partial}{\partial z} \left[\sum_{i=0}^1 \bar{F}_i \right]$ in Eqs. (1)
278 and (5). We conducted another sensitivity test where all parameters are identical to those in the HL model
279 except that G in both the control and experimental runs is twice as large as that used by HL. As the
280 radiative damping profile changes from the black line to the red line above 24 km shown in FIG. 1
281 meanwhile the Brunt-Väisälä frequency is decreased by 2.5% in the experimental run, our simulated
282 QBO period decreases from 28.4 months to 27.6 months (figures not shown). This smaller percentage



283 decrease of 2.8% is not unexpected because the unrealistically larger G that is independent of \bar{u} makes
284 the model atmosphere less sensitive to the changes in the radiative damping.

285 We further conducted two sensitivity tests where all parameters are identical to those in the HL model
286 except that G in the first test is half as large as that used by HL and is equal to zero in the second test.
287 Surprisingly, as the radiative damping profile changes from the black line to the red line above 24 km
288 shown in FIG. 1 while the Brunt-Väisälä frequency is decreased by 2.5% in the experimental runs, our
289 simulated QBO periods decreases from 30.0 months to 28.6 months both for G being decreased by 50%
290 and for $G = 0$. This 4.7% decrease in the QBO period is identical to the reduction obtained from the
291 sensitivity test presented in section 2 when G is the same as that used by HL. The question naturally
292 arises: what is responsible for this unphysical behavior?

293 Plumb (1977) pointed out that the upper boundary in HL was undesirably low and implied that raising
294 the lid to an additional 50% would be adequate for the robustness in his model. Here, we carry out a
295 series of sensitivity tests by raising the model lid gradually from 35 km to 55 km with the one-kilometer
296 increment. we will demonstrate how the behavior of the HL model with $G = 0$ converges with that of
297 the Plumb model. The modified HL model, i.e., the HL model with $G = 0$ is identical to the Plumb
298 model except that the former has the no-slip upper boundary condition while the latter has the stress-free
299 upper boundary condition. Both models share the same governing equation (5). Note that we set the
300 radiative damping rate above the 35 km level to its value at the 35 km level shown in FIG. 1.

301 For the radiative damping profile corresponding to the reference CO_2 , FIG. 6 shows that the simulated
302 QBO period with the no-slip upper boundary condition (solid black line) is 30.0 months when the model
303 lid is placed at 35 or 36 km level; 30.8 months when the model lid is placed at 37, 38, or 39 km level;
304 31.6 months when the model lid is placed between the 40 and 45 km levels; 32.4 months when the model
305 lid is placed at or above the 46 km level while the simulated QBO period with the stress-free upper



306 boundary condition (dashed black line in FIG. 6) decreases from 37.5 to 35.5 months as the model lid is
307 raised from the 35 to 36 km level; continues decreasing to 34.3 and 33.3 months as the model lid is raised
308 to 37 and 38 km level, respectively; is kept at 33.3 months when the model lid is placed between the 38
309 and 41 km levels; and it further decreases to 32.4 months when the model lid is placed at or above the
310 42 km level. No matter whether we adopt the no-slip or stress-free upper boundary condition, the
311 simulated QBO period is 32.4 months for the reference radiative damping profile provided that the model
312 top is at or above the 46 km level.

313 Similarly, for the radiative damping profile corresponding to the doubled CO₂, FIG. 6 shows that the
314 simulated QBO period with the no-slip upper boundary condition (solid red line) is 28.6 months when
315 the model lid is placed at 35 km level; 29.3 months when the model lid is placed at 36, 37, or 38 km
316 level; 30.0 months when the model lid is placed at or above the 39 km level while the simulated QBO
317 period with the stress-free upper boundary condition (dashed red line in FIG. 6) decreases from 31.6 to
318 30.8 months as the model lid is raised from the 35 to 36 km level; and is kept at 30.0 months when the
319 model lid is placed at or above to 37 km level. No matter whether we adopt the no-slip or stress-free
320 upper boundary condition, the simulated QBO period for the enhanced infrared cooling due to the
321 doubled CO₂ is 30.0 months provided that the model top is at or above the 39 km level. It is apparent
322 that the required model top is lower when the radiative damped is augmented because the planetary
323 waves dissipate more steeply with height in presence of the enhanced infrared cooling rates.

324 FIG. 6 demonstrates that when the model lid is sufficiently high the response of the QBO period to
325 the enhanced radiative damping due to the increasing CO₂ will decrease from 32.4 to 30.0 months. This
326 7.4% decrease in the QBO period is independent of the upper boundary condition.

327

328 **5. Conclusions**



329 Plumb (1977) envisioned that stratospheric climate change would give rise to long-term changes in
330 the QBO period due to changes in radiative damping and the Brunt-Väisälä frequency. Using one-
331 dimensional (1D) models we found that the enhanced radiative damping arising from the doubling of
332 CO₂ leads to the shortening of the QBO period by about 7.4% provided that the model top is higher than
333 the 46 km level. Those models include neither gravity waves nor tropical upwelling and assume that
334 there are no changes in wave fluxes entering the equatorial stratosphere.

335 From a comprehensive model perspective, Richter et al. (2020b) showed that the changes in period
336 of the QBO in warming climate simulations varied quite significantly among these models. Some models
337 projected longer mean periods and some shorter mean periods for the QBO in a future warmer climate.
338 They argue that uncertainty in the representation of the parameterized gravity waves is the most likely
339 cause of the spread among the QBOi models in the QBO's response to climate change.

340 In addition, CO₂ increases in the NASA Goddard Institute for Space Studies Model E2.2-AP (Rind
341 et al. 2020) lead to a decrease of both QBO period and QBO amplitude (DallaSanta et al., in prep.). The
342 period decrease is associated with increases in lower stratospheric momentum fluxes (related to
343 parameterized convection), a finding consistent with Geller et al. (2016) and Richter et al. (2020b). The
344 amplitude decrease is associated with a strengthened residual mean circulation, also consistent with the
345 literature, although the vertical structure of the circulation response is nontrivial.

346 Our 1D models only explored how the QBO period responds to the enhancing radiative damping of
347 planetary waves due to the increasing CO₂. In order to investigate how the enhancing radiative damping
348 impacts on gravity waves which play an even more important role in determining the QBO period than
349 planetary waves, high-resolution models such as those used by Kawatani et al. (2011, 2019) are desirable
350 to further our understanding. Ultimately, how the QBO period changes in response to the increasing CO₂
351 will be determined by the combined effects of the strengthening of tropical upwelling, the increasing of



352 wave fluxes entering the equatorial stratosphere, and the enhancing of radiative damping, which warrants
353 further research.

354
355 **Acknowledgements:** Climate modeling at GISS is supported by the NASA Modeling, Analysis and
356 Prediction program, and resources supporting this work were provided by the NASA High-End
357 Computing (HEC) Program through the NASA Center for Climate Simulation (NCCS) at Goddard
358 Space Flight Center. KD acknowledges support from the NASA Postdoctoral Program. The authors
359 also acknowledge very useful discussions with Drs. Geller and Clara Orbe.

360

361 **References**

362

363 Andrews, D. G., Holton, J. R., and Leovy, C. B.: Middle Atmosphere Dynamics, Academic Press, 489
364 pp, 1987.

365 Baldwin, M. P., Gray, L. J., Dunkerton, T. J., Hamilton, K., Haynes, P. H., Randel, W. J., Holton, J. R.,
366 Alexander, M. J., Hirota, I., Horinouchi, T., Jones, D. B. A., Kinnersley, J. S., Marquardt, C., Sato,
367 K., and Takahashi, M.: The Quasi-biennial oscillation, *Rev. Geophys.*, 39, 179–229,
368 <https://doi.org/10.1029/1999RG000073>, 2001.

369 Butchart, N., Scaife, A. A., Bourqui, M., Grandpré, J., Hare, S. H., Kettleborough, J., Langematz, U.,
370 Manzini, E., Sassi, F., Shibata, K., Shindell, D. and Sigmond, M.: Simulations of anthropogenic
371 change in the strength of the Brewer–Dobson circulation, *Climate Dynamics*, 27, 727–741,
372 <https://doi.org/10.1007/s00382-006-0162-4>, 2006.

373 Butchart, N., Anstey, J., Hamilton, K., Osprey, S., McLandress, C., Bushell, A. C., Kawatani, Y., Kim,
374 Y.-H., Lott, F., Scinocca, J., Stockdale, T.N., Andrews, M., Bellprat, O., Braesicke, P., Cagnazzo,
375 C., Chen, C.-C., Chun, H.-Y., Dobrynin, M., Garcia, R., Garcia-Serrano, J., Gray, L.J., Holt, L.,
376 Kerzenmacher, T., Naoe, H., Pohlmann, H., Richter, J. H., Scaife, A.A., Schenzinger, V., Serva, F.,



- 377 Versick, S., Watanabe, S., Yoshida, K. and Yukimoto, S.: Overview of experiment design and
378 comparison of models participating in phase 1 of the SPARC Quasi-Biennial Oscillation initiative
379 (QBOi), *Geoscientific Model Development*, 11, 1009–1032. [https://doi.org/10.5194/gmd-11-1009-](https://doi.org/10.5194/gmd-11-1009-2018)
380 [2018](https://doi.org/10.5194/gmd-11-1009-2018), 2018.
- 381 Butchart, N., Anstey, J. A., Kawatani, Y., Osprey, S. M., Richter, J. H., Wu, T.: QBO changes in CMIP6
382 climate projections, *Geophys. Res. Lett.*, 47, 1–10. <https://doi.org/10.1029/2019GL086903>, 2020.
- 383 Camargo, S. J. and Sobel, A. H.: Revisiting the influence of the quasi-biennial oscillation on tropical
384 cyclone activity, *J. Climate*, 23, 5810–5825, <https://doi.org/10.1175%2F2010JCLI3575.1>, 2010.
- 385 Collimore, C. C., Martin, D. W., Hitchman, M. H., Huesmann, A., and Waliser, D. E.: On the
386 relationship between the QBO and tropical deep convection, *J. Climate*, 16, 2552–2568,
387 [https://doi.org/10.1175/1520-0442\(2003\)016%3C2552:OTRBTQ%3E2.0.CO;2](https://doi.org/10.1175/1520-0442(2003)016%3C2552:OTRBTQ%3E2.0.CO;2), 2003.
- 388 Ebdon, R. A.: Notes on the wind flow at 50mb in tropical and subtropical regions in January 1957 and in
389 1958, *Q. J. Roy. Meteor. Soc.*, 86, 540–542, <https://doi.org/10.1002/qj.49708637011>, 1960.
- 390 Fels, S. B.: A parameterization of scale-dependent radiative damping rates in the middle atmosphere, *J.*
391 *Atmos. Sci.*, 39, 1141–1152, [https://doi.org/10.1175/1520-](https://doi.org/10.1175/1520-0469(1982)039%3C1141:APOSDR%3E2.0.CO;2)
392 [0469\(1982\)039%3C1141:APOSDR%3E2.0.CO;2](https://doi.org/10.1175/1520-0469(1982)039%3C1141:APOSDR%3E2.0.CO;2), 1982.
- 393 Fels, S. B.: Radiative-dynamical interactions in the middle atmosphere, *Advances in Geophysics*, Vol.
394 28A, Academic Press, 277–300, [https://doi.org/10.1016/S0065-2687\(08\)60227-7](https://doi.org/10.1016/S0065-2687(08)60227-7), 1985.
- 395 Garfinkel, C. I. and Hartmann, D. L.: The influence of the quasi-biennial oscillation on the troposphere
396 in winter in a hierarchy of models. Part I: Simplified dry GCMs, *J. Atmos. Sci.*, 68, 1273–1289,
397 <https://doi.org/10.1175%2F2011JAS3665.1>, 2011a.



- 398 Garfinkel, C. I. and Hartmann, D. L.: The influence of the quasi-biennial oscillation on the troposphere
399 in winter in a hierarchy of models. Part II: Perpetual winter WACCM runs, *J. Atmos. Sci.*, 68, 2026–
400 2041, <https://doi.org/10.1175%2F2011JAS3702.1>, 2011b.
- 401 Geller, M. A., Zhou, T., Shindell, D., Ruedy, R., Aleinov, I., Nazarenko, L., Tausnev, N. L., Kelley, M.,
402 Sun, S., Cheng, Y., Field, R. D., and Faluvegi, G.: Modeling the QBO-improvements resulting from
403 higher-model vertical resolution, *J. Adv. Model. Earth Syst.*, 8, 1092–1105,
404 <https://doi.org/10.1002/2016MS000699>, 2016.
- 405 Gidden, M. J., Riahi, K., Smith, S. J., Fujimori, S., Luderer, G., Kriegler, E., van Vuuren, D. P., van den
406 Berg, M., Feng, L., Klein, D., Calvin, K., Doelman, J. C., Frank, S., Fricko, O., Harmsen, M.,
407 Hasegawa, T., Havlik, P., Hilaire, J., Hoesly, R., Horing, J., Popp, A., Stehfest, E., and Takahashi,
408 K.: Global emissions pathways under different socioeconomic scenarios for use in CMIP6: a dataset
409 of harmonized emissions trajectories through the end of the century, *Geosci. Model Dev.*, 12, 1443–
410 1475, <https://doi.org/10.5194/gmd-12-1443-2019>, 2019.
- 411 Giorgetta, M. A. and Doege, M. C.: Sensitivity of the Quasi-Biennial Oscillation to CO₂ doubling,
412 *Geophys. Res. Lett.*, 32, L08701. <https://doi.org/10.1029/2004GL021971>, 2005.
- 413 Giorgetta, M. A., Bengtson, L., and Arpe, K.: An investigation of QBO signals in the east Asian and
414 Indian monsoon in GCM experiments, *Climate Dynamics*, 15, 435–450,
415 <https://doi.org/10.1007/s003820050292>, 1999.
- 416 Giorgetta, M. A., Manzini, E., and Roeckner, E.: Forcing of the quasi-biennial oscillation from a broad
417 spectrum of atmospheric waves, *Geophys. Res. Lett.*, 29, <https://doi.org/10.1029/2002GL014756>,
418 2002.



- 419 Giorgetta, M. A., Manzini, E., and Roeckner, E., Esch, M., and Bengtsson, L.: Climatology and forcing
420 of the quasi-biennial oscillation in the MAECHM5 model, *J. Climate*, 19, 3882–3901,
421 <https://doi.org/10.1175/JCLI3830.1>, 2006.
- 422 Gray, W. M.: Atlantic seasonal hurricane frequency. Part I: El Niño and 30-mb quasi-biennial oscillation
423 influences, *Mon. Wea. Rev.*, 112, 1649–1688, [https://doi.org/10.1175/1520-
424 0493\(1984\)112%3C1649:ASHFPI%3E2.0.CO;2](https://doi.org/10.1175/1520-0493(1984)112%3C1649:ASHFPI%3E2.0.CO;2), 1984.
- 425 Gray, W. M., Sheaffer, J. D., and Knaff, J.: Influence of the stratospheric QBO on ENSO variability, *J.*
426 *Meteor. Soc. Jpn.*, 70, 975–995, https://doi.org/10.2151/jmsj1965.70.5_975, 1992.
- 427 Hamilton, K.: The vertical structure of the quasi-biennial oscillation: Observations and theory, *Atmos.*
428 *Ocean*, 19, 236–250, <http://dx.doi.org/10.1080/07055900.1981.9649111>, 1981.
- 429 Hansen, F., Matthes, K., and Wahl, S.: Tropospheric QBO–ENSO interactions and differences between
430 the Atlantic and Pacific, *J. Climate*, 29, 1353–1368, <https://doi.org/10.1175/JCLI-D-15-0164.1>,
431 2016
- 432 Hasebe, F.: Quasi-biennial oscillations of ozone and diabatic circulation in the equatorial stratosphere, *J.*
433 *Atmos. Sci.*, 51, 729–745, [https://doi.org/10.1175/1520-
434 0469\(1994\)051%3c0729:QBOOOA%3e2.0.CO;2](https://doi.org/10.1175/1520-0469(1994)051%3c0729:QBOOOA%3e2.0.CO;2), 1994.
- 435 Hitchman, M. H., and Huesmann, A. S.: Seasonal influence of the quasi-biennial oscillation on
436 stratospheric jets and Rossby wave breaking, *J. Atmos. Sci.*, 66, 935–946,
437 <https://doi.org/10.1175%2F2008JAS2631.1>, 2009.
- 438 Ho, C.-H., Kim, H.-S., Jeong, J.-H., and Son, S.-W.: Influence of stratospheric quasi-biennial oscillation
439 on tropical cyclone tracks in the western North Pacific, *Geophys. Res. Lett.*, 36, L06702,
440 <http://dx.doi.org/10.1029/2009GL037163>, 2009.



- 441 Holt, L., Lott, F., Garcia, R., Kiladis, G.N., Anstey, J.A., Braesicke, P., Bushell, A.C., Butchart, N.,
442 Cagnazzo, C., Chen, C.-C., Chun, H.-Y., Hamilton, K., Kawatani, Y., Kerzenmacher, T., Kim, Y.-
443 H., McLandress, C., Naoe, H., Osprey, S., Richter, J.H., Scinocca, J., Serva, F., Versick, S.,
444 Watanabe, S., Yoshida, K., and Yukimoto, S.: An evaluation of tropical waves and wave forcing of
445 the QBO in the QBOi models, *Q. J. R. Meteorol. Soc.*, <https://doi.org/10.1002/qj.3827>, 2020.
- 446 Holton, J. R. and Lindzen, R. S.: An updated theory for the quasi-biennial cycle of the tropical
447 stratosphere, *J. Atmos. Sci.*, 29, 1076–1080, [https://doi.org/10.1175/1520-0469\(1972\)029%3c1076:AUTFTQ%3e2.0.CO;2](https://doi.org/10.1175/1520-0469(1972)029%3c1076:AUTFTQ%3e2.0.CO;2), 1972.
- 449 Holton, J. R. and Tan, H.: The Influence of the equatorial quasi-biennial oscillation on the global
450 circulation at 50 mb, *J. Atmos. Sci.*, 37, 2200–2208, [https://doi.org/10.1175/1520-0469\(1980\)037%3c2200:TIOTEQ%3e2.0.CO;2](https://doi.org/10.1175/1520-0469(1980)037%3c2200:TIOTEQ%3e2.0.CO;2), 1980.
- 452 Huang, B. H., Hu, Z. Z., Kinter, J. L., Wu, Z. H., and Kumar, A.: Connection of stratospheric QBO with
453 global atmospheric general circulation and tropical SST. Part I: Methodology and composite life
454 cycle, *Climate Dynamics*, 38, 1–23, <https://doi.org/10.1007%2Fs00382-011-1250-7>, 2012.
- 455 Kawatani, Y. and Hamilton, K.: Weakened stratospheric Quasi-Biennial Oscillation driven by increased
456 tropical mean upwelling, *Nature*, 497, 478–481, <https://doi.org/10.1038/nature12140>, 2013.
- 457 Kawatani, Y., Takahashi, M., Sato, K., Alexander, S. P., and Tsuda, T.: Global distribution of
458 atmospheric waves in the equatorial upper troposphere and lower stratosphere: AGCM simulation
459 of sources and propagation, *J. Geophys. Res.*, 114, D01102, <https://doi.org/10.1029/2008JD010374>,
460 2009.
- 461 Kawatani, Y., Watanabe, S., Sato, K., Dunkerton, T. J., Miyahara, S., and Takahashi, M.: The roles of
462 equatorial trapped waves and internal inertia-gravity waves in driving the Quasi-Biennial oscillation.



- 463 Part I: Zonal mean wave forcing, *J. Atmos. Sci.*, 67, 963–980,
464 <https://doi.org/10.1175/2009JAS3222.1>, 2010.
- 465 Kawatani, Y., Hamilton, K., and Watanabe, S.: The quasi-biennial oscillation in a double CO₂ climate,
466 *J. Atmos. Sci.*, 68, 265–283, <https://doi.org/10.1175/2010JAS3623.1>, 2011.
- 467 Kawatani, Y., Lee, J. N., and Hamilton, K.: Interannual variations of stratospheric water vapor in MLS
468 observations and climate model simulations, *J. Atmos. Sci.*, 71, 4072–4085,
469 <https://doi.org/10.1175/JAS-D-14-0164.1>, 2014.
- 470 Kawatani, Y., Hamilton, K., Sato, K., Dunkerton, T. J., Watanabe, S., and Kikuchi, K.: ENSO Modulation
471 of the QBO: Results from MIROC Models with and without Nonorographic Gravity Wave
472 Parameterization, *J. Atmos. Sci.*, 76, 3893–3917, <https://doi.org/10.1175/JAS-D-19-0163.1>, 2019.
- 473 Labitzke, K.: On the interannual variability of the middle stratosphere during the northern winters, *J.*
474 *Meteorol. Soc. Jpn.*, 80, 963–971, http://doi.org/10.2151/jmsj1965.60.1_124, 1982.
- 475 Lait, L. R., Schoeberl, M. R., and Newman, P. A.: Quasi-biennial modulation of the Antarctic ozone
476 depletion, *J. Geophys. Res.*, 94, 11559–11571, <http://dx.doi.org/10.1029/JD094iD09p11559>, 1989.
- 477 Li, F., Austin, J., and Wilson, R. J.: The strength of the Brewer–Dobson circulation in a changing climate:
478 Coupled chemistry–climate model simulations, *J. Climate*, 21, 40–57,
479 <https://doi.org/10.1175/2007JCLI1663.1>, 2008.
- 480 Liess, S. and Geller, M. A.: On the relationship between QBO and distribution of tropical deep
481 convection, *J. Geophys. Res.*, 117, D03108, <http://dx.doi.org/10.1029/2011JD016317>, 2012.
- 482 Lindzen, R. S.: Equatorial planetary waves in shear: Part I, *J. Atmos. Sci.* 28, 609–622,
483 [https://doi.org/10.1175/1520-0469\(1971\)028%3C0609:EPWISP%3E2.0.CO;2](https://doi.org/10.1175/1520-0469(1971)028%3C0609:EPWISP%3E2.0.CO;2), 1971.
- 484 Lindzen, R. S. and Holton, J. R.: A theory of the quasi-biennial oscillation, *J. Atmos. Sci.*, 25, 1095–
485 1107, [https://doi.org/10.1175/1520-0469\(1968\)025%3C1095:ATOTQB%3E2.0.CO;2](https://doi.org/10.1175/1520-0469(1968)025%3C1095:ATOTQB%3E2.0.CO;2), 1968.



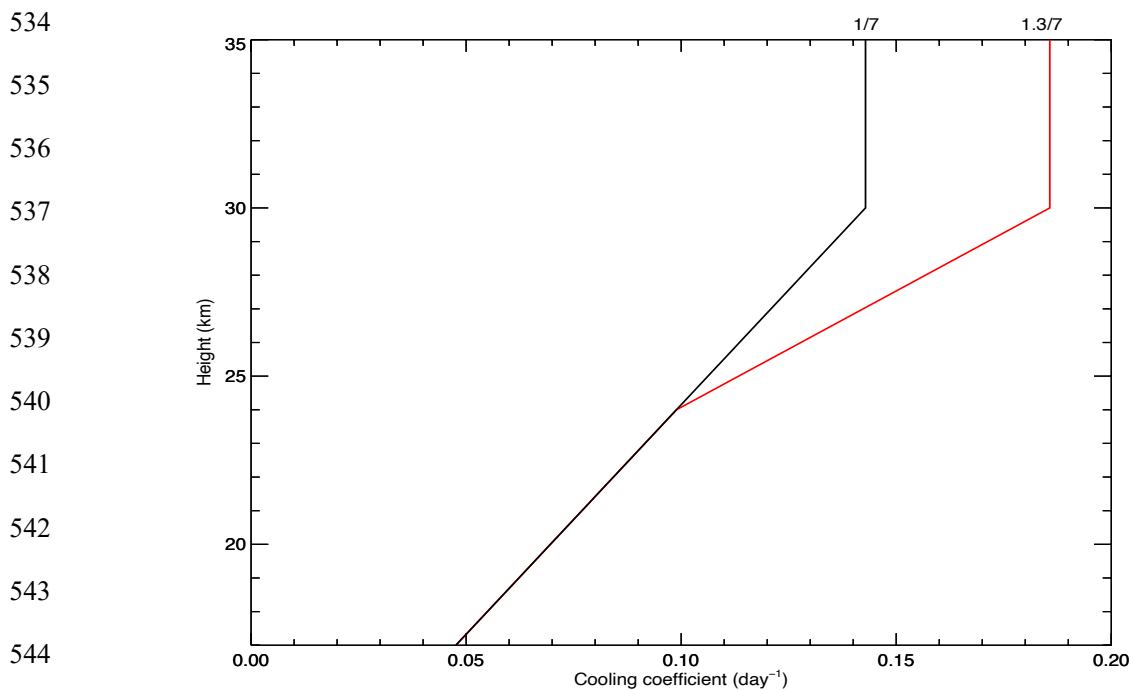
- 486 Marshall, A. G. and Scaife, A. A.: Impact of the QBO on surface winter climate, *J. Geophys. Res.*, 114,
487 D18110, <http://dx.doi.org/10.1029/2009JD011737>, 2009.
- 488 Matsuno, T.: Numerical integrations of primitive equations by use of a simulated backward difference
489 method, *J. Meteor. Soc. Japan*, 44, 76–84, https://doi.org/10.2151/jmsj1965.44.1_76, 1966
- 490 Plass, G. N.: The influence of the 15μ carbon-dioxide band on the atmospheric infra-red cooling rate,
491 *Quart. J. Roy. Meteor. Soc.*, 82, 310–324, <https://doi.org/10.1002/qj.49708235307>, 1956.
- 492 Plumb, R. A.: The interaction of two internal waves with the mean flow: Implications for the theory of
493 the quasi-biennial oscillation, *J. Atmos. Sci.*, 34, 1847–1858,
494 <https://doi.org/10.1002/qj.49708235307>, 1977.
- 495 Reed, R. J., Campbell, W. J., Rasmussen, L. A., and Rogers, D. G.: Evidence of a downward-propagating,
496 annual wind reversal in the equatorial stratosphere, *J. Geophys. Res.*, 66, 813–818,
497 <http://dx.doi.org/10.1029/JZ066i003p00813>, 1961.
- 498 Richter, J. H., Anstey, J. A., Butchart, N., Kawatani, Y., Meehl, G. A., Osprey, S., & Simpson, I. R.,
499 2020b: Progress in simulating the quasi-biennial oscillation in CMIP models. *Journal Geophysical*
500 *Research: Atmospheres*, 125, e2019JD032362, <https://doi.org/10.1029/2019JD032362>, 2020a.
- 501 Richter, J. H., Butchart, N., Kawatani, Y., Bushell, A. C., Holt, L., Serva, F., Anstey, J., Simpson, I. R.,
502 Osprey, S., Hamilton, K., Braesicke, P., Cagnazzo, C., Chen, C.-C., Garcia, R. R., Gray, L. J.,
503 Kerzenmacher, T., Lott, F., McLandress, C., Naoe, H., Scinocca, J., Stockdale, T. N, Versick, S.,
504 Watanabe, S., Yoshida, K., Yukimoto, S.: Response of the Quasi-Biennial Oscillation to a warming
505 climate in global climate models, *Q. J. R. Meteorol. Soc.*, 1–29. <https://doi.org/10.1002/qj.3749>,
506 2020b.



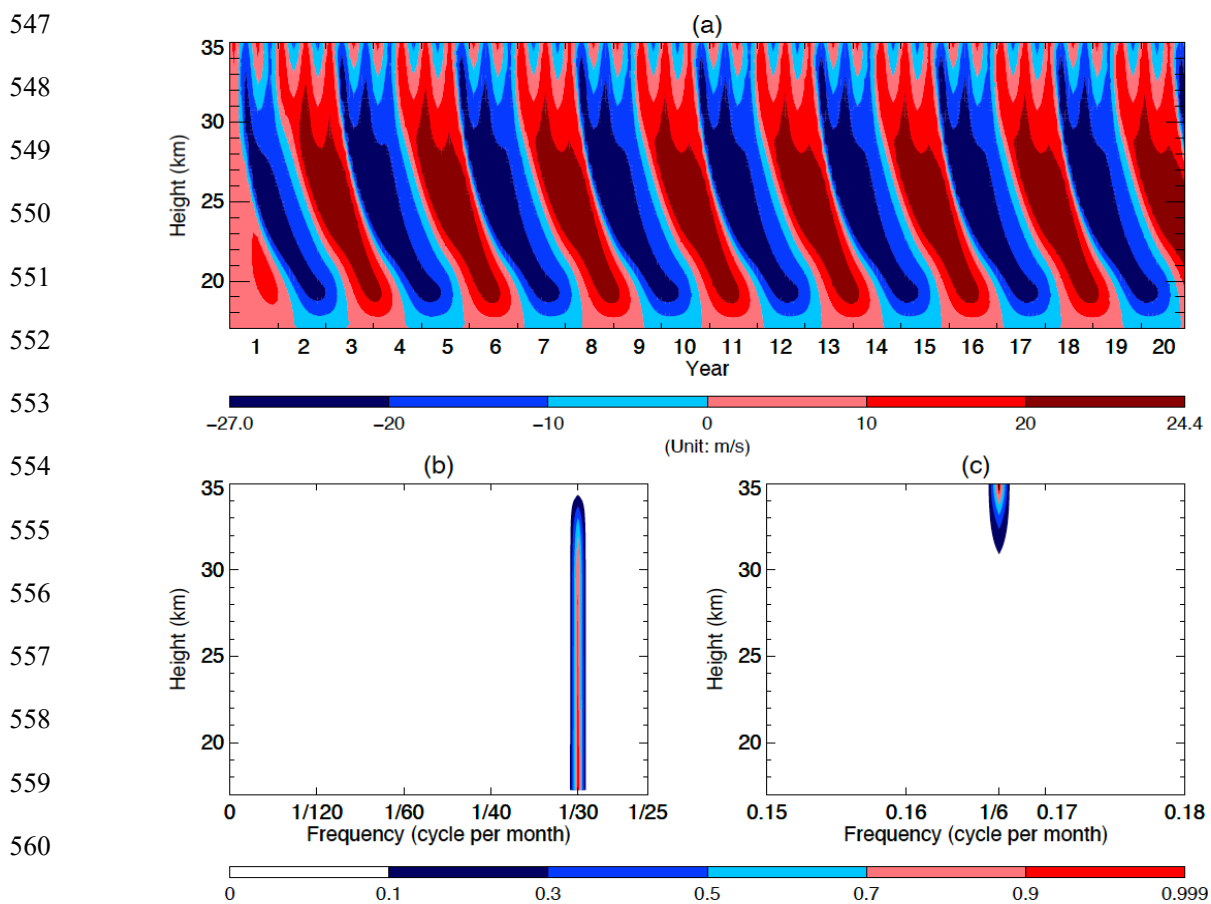
- 507 Rind, D., Jonas, J., Balachandran, N., Schmidt, G., and Lean, J.: The QBO in two GISS global climate
508 models: 1. Generation of the QBO, *J. Geophys. Res. Atmos.*, 119, 8798–8824,
509 <https://doi.org/10.1002/2014JD021678>, 2014.
- 510 Rind, D., Orbe, C., Jonas, J., Nazarenko, L., Zhou, T., Kelley, M., Lacis, A., Shindell, D., Faluvegi,
511 Russell, G., Bauer, M., Schmidt, G., Romanou, A., and Tausnev, N.: GISS Model E2.2: A climate
512 model optimized for the middle atmosphere — Model structure, climatology, variability and climate
513 sensitivity, *J. Geophys. Res. Atmos.*, 125, e2019JD032204, <https://doi.org/10.1029/2019JD032204>,
514 2020.
- 515 Saravanan, R.: A multiwave model of the quasi-biennial oscillation, *J. Atmos. Sci.*, 47, 2465–2474,
516 doi:[10.1175/1520-0469\(1990\)047<2465:AMMOTQ>2.0.CO;2](https://doi.org/10.1175/1520-0469(1990)047<2465:AMMOTQ>2.0.CO;2), 1990.
- 517 Scaife, A. A., Butchart, N., Warner, C. D., Stainforth, D., Norton, W., and Austin, J.: Realistic quasi-
518 biennial oscillations in a simulation of the global climate, *Geophys. Res. Lett.*, 27, 3481–3484,
519 <https://doi.org/10.1029/2000GL011625>, 2000.
- 520 Schirber, S., Manzini, E., Krismer, T. and Giorgetta, M.: The Quasi-Biennial Oscillation in a warmer
521 climate: sensitivity to different gravity wave parameterizations, *Climate Dynamics*, 45, 825–
522 836, <https://doi.org/10.1007/s00382-014-2314-2>, 2015.
- 523 Trepte, C. R. and Hitchman, M. H.: Tropical stratospheric circulation deduced from satellite aerosol data,
524 *Nature*, 355, 626–628, <https://doi.org/10.1038/355626a0>, 1992.
- 525 Watanabe, S. and Kawatani, Y.: Sensitivity of the QBO to mean tropical upwelling under a changing
526 climate simulated with an Earth System Model, *Journal of the Meteorological Society of Japan*,
527 Series II, 90A, 351–360, <https://doi.org/10.2151/jmsj.2012-A20>, 2012.



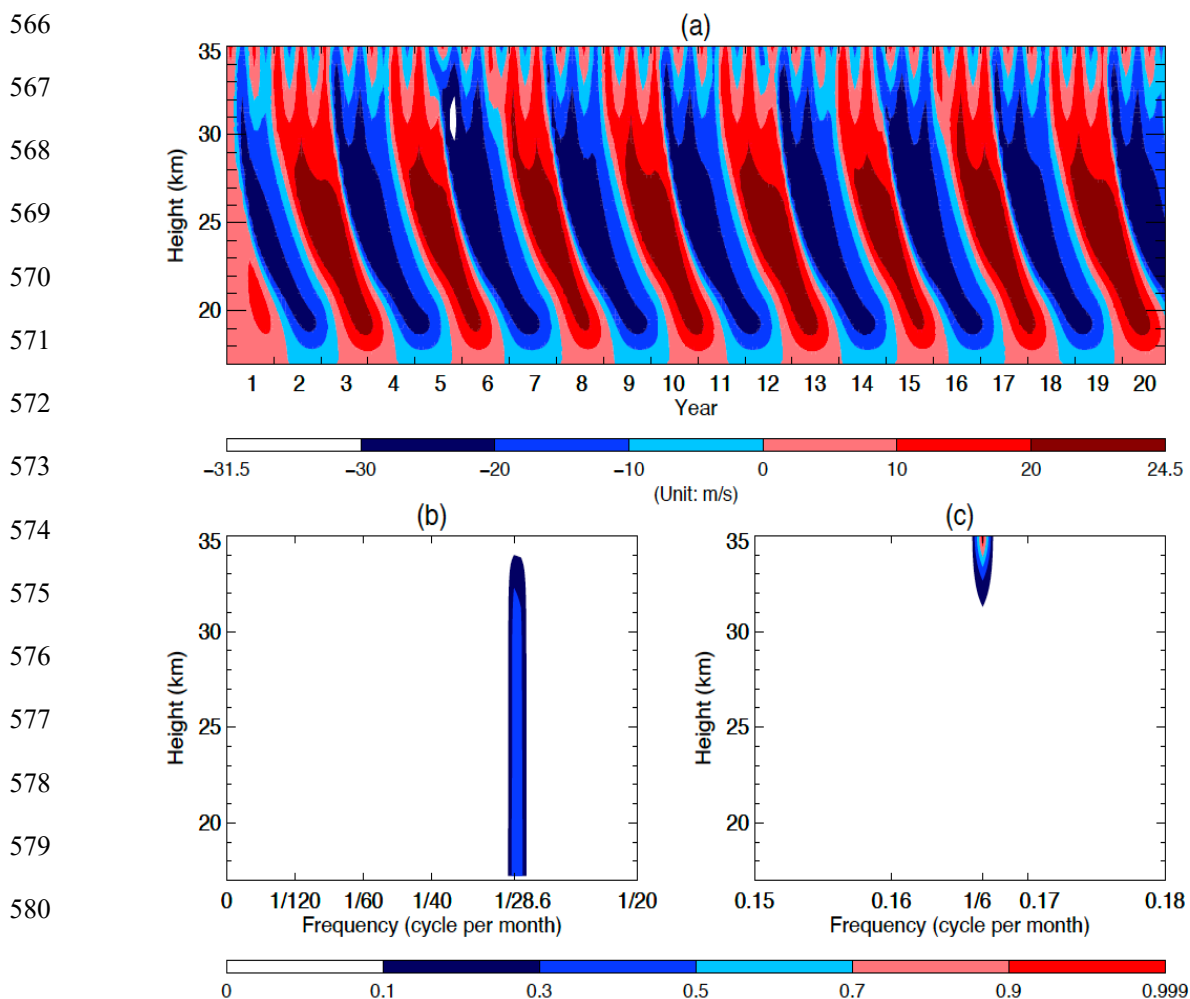
- 528 Yoo, C. and Son, S.-W.: Modulation of the boreal wintertime Madden-Julian oscillation by the
529 stratospheric quasi-biennial oscillation, *Geophys. Res. Lett.*, 43, 1392–1398,
530 <https://doi.org/10.1002%2F2016GL067762>, 2016.
- 531 Zawodny, J. M. and McCormick, M. P.: Stratospheric Aerosol and Gas Experiment II measurements of
532 the quasi-biennial oscillations in ozone and nitrogen dioxide, *J. Geophys. Res.*, 96, 9371– 9377,
533 <http://dx.doi.org/10.1029/91JD00517>, 1991.



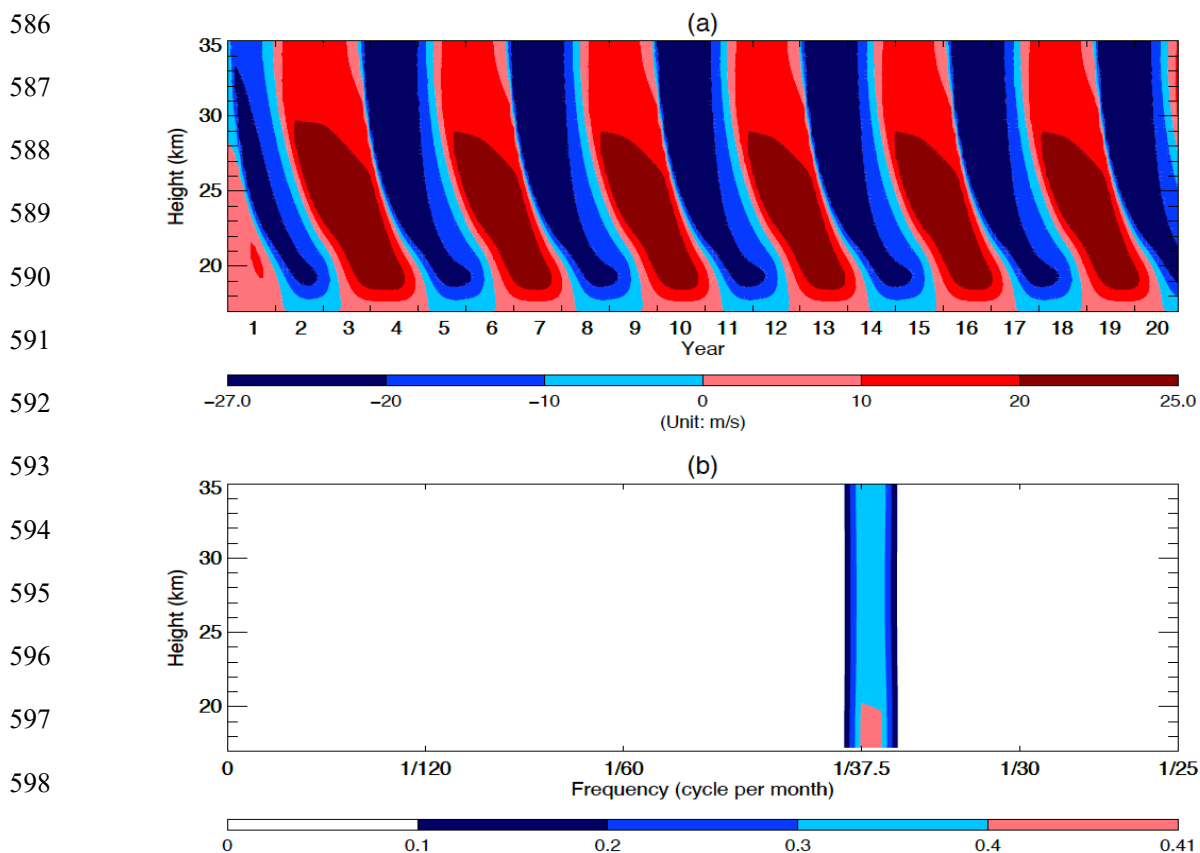
545 **FIG. 1:** Newtonian cooling profiles: The smaller values (black line) are used for the control runs while
546 the larger values (red line) are used for the experimental runs.



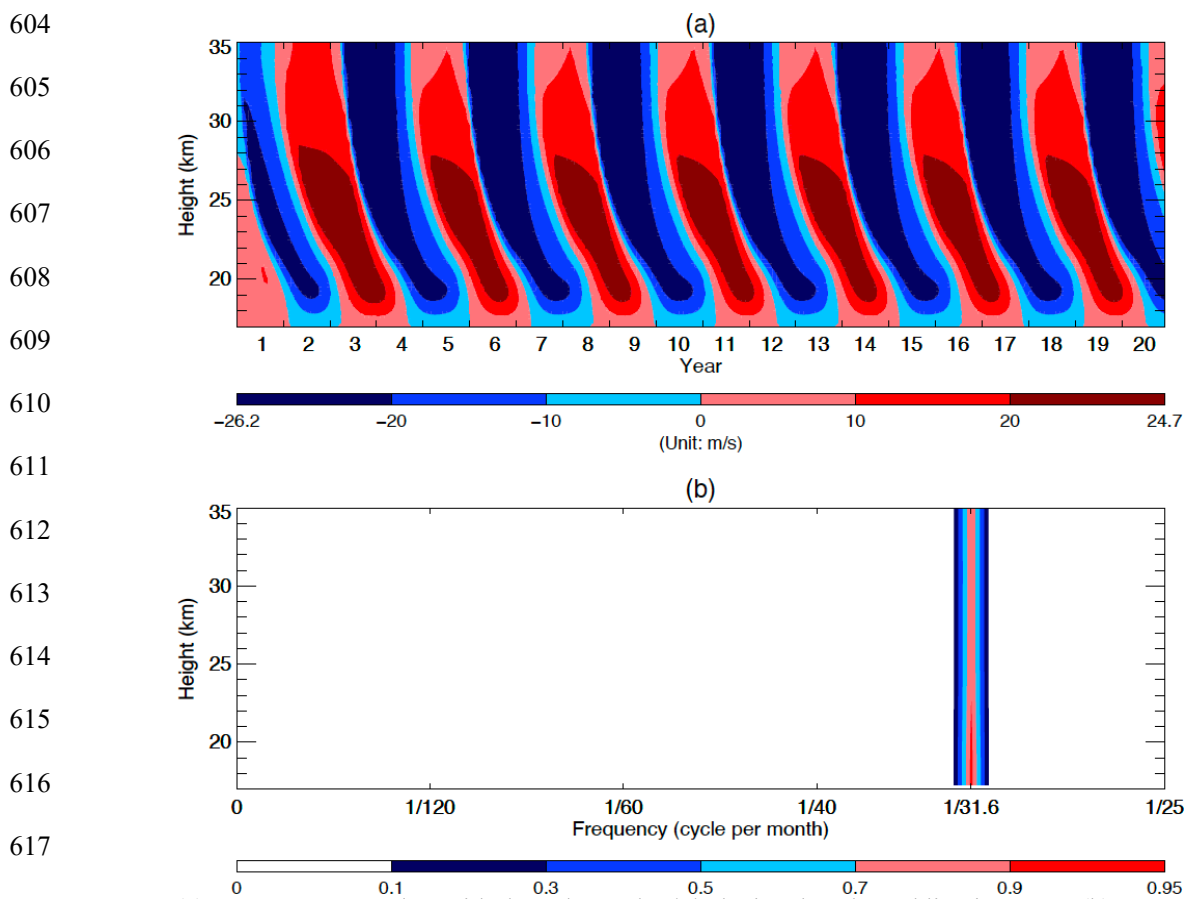
561 **FIG. 2:** (a) Time–height section of the monthly averaged mean zonal wind over the first 20 years from
562 the HL’s original model. (b) and (c) Frequency–height section of the power spectral densities (PSD) of
563 the standardized monthly averaged mean zonal wind of the 100 years. Note that in order to better
564 visualize the PSD in (b) and (c), we trimmed off the blank segments for the frequencies ranging from
565 $\frac{1}{25}$ to 0.15 cycle per month and those ranging from 0.18 to 0.5 cycle per month.



581 **FIG. 3:** (a) Same as FIG. 2a, but with the enhanced $\alpha(z)$ depicted as the red line in FIG. 1. (b) and (c)
582 Frequency–height section of the power spectral densities (PSD) of the standardized monthly averaged
583 mean zonal wind of the 100 years. Note that in order to better visualize the PSD in (b) and (c), we
584 trimmed off the blank segments for the frequencies ranging from $\frac{1}{20}$ to 0.15 cycle per month and those
585 ranging from 0.18 to 0.5 cycle per month.



599 **FIG. 4:** (a) Time–height section of the monthly averaged mean zonal wind over the first 20 years from
600 the HL’s model without the semiannual forcing. (b) Frequency–height section of the power spectral
601 densities (PSD) of the standardized monthly averaged mean zonal wind of the 100 years. Note that in
602 order to visualize the PSD, we trimmed off the blank segment for the frequencies ranging from $\frac{1}{25}$ to
603 0.5 cycle per month.



618 **FIG. 5:** (a) Same as FIG. 4a, but with the enhanced $\alpha(z)$ depicted as the red line in FIG. 1. (b) Same as
619 FIG. 4b, but for the doubled CO₂ Run.



620

621

622

623

624

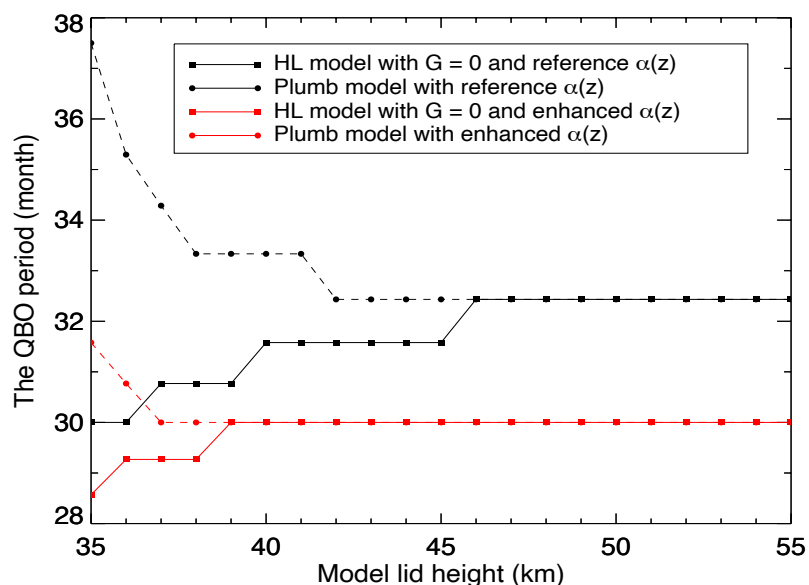
625

626

627

628

629



630

631

632

633

FIG. 6: The relationship between the simulated QBO period with the height of the model lid. Black and red lines depict the results from using the reference radiative damping and the enhanced radiative damping respectively while solid and dashed lines delineate the results from the HL model with $G = 0$ and the Plumb model respectively.